JOURNAL OF AIRCRAFT
Vol. 52, No. 1, January–February 2015

Boundary-Layer Stability Analysis of the Mean Flows Obtained Using Unstructured Grids

Wei Liao*
National Institute of Aerospace, Hampton, Virginia 23666
and
Mujeeb R. Malik,† Elizabeth M. Lee-Rausch,‡ Fei Li,§ Eric J. Nielsen,¶ Pieter G. Buning,**
Meelan Choudhari,†† and Chau-Lyan Chang‡‡
NASA Langley Research Center, Hampton, Virginia 23681

DOI: 10.2514/1.C032583

Boundary-layer stability analyses of mean flows extracted from unstructured-grid Navier–Stokes solutions have been performed. A procedure has been developed to extract mean flow profiles from the FUN3D unstructured-grid solutions for the purpose of stability analysis. Extensive code-to-code validations were performed by comparing the extracted mean flows as well as the corresponding stability characteristics to the predictions based on structured-grid mean flow solutions. Comparisons were made for a set of progressively complex geometric configurations ranging from a simple flat plate to a full aircraft configuration: a modified Gulfstream III with a natural laminar-flow glove. The results for the swept wing flow over the wing–glove assembly point to the need for stability analysis based on Navier–Stokes solutions or possibly fully three-dimensional boundary-layer codes when the underlying flow develops strong three-dimensionality. The effect of grid resolution, mean flow convergence, and low-order interpolation to a stability grid on metrics relevant to linear stability of the boundary-layer flow are also examined to provide guidelines for the use of both structured and unstructured grids in practical applications related to transition prediction for swept wing boundary layers.

Nomenclature

C	=	wing/airfoil chord length
C_p	=	pressure coefficient
f	=	disturbance frequency
H	=	flight altitude
N	=	ln(current disturbance amplitude/initial disturbance amplitude)
R_{CF}	=	$\lvert U_{C\ \max}\rvert\delta_{01}/\nu_e$; crossflow Reynolds number
Re	=	freestream Reynolds number
Re_y	=	$U_e x/\nu_e$, Reynolds number based on the local boundary-layer edge velocity
r_1	=	geometric stretching rate used in VGRID
r_2	=	modifier to r_1, used to tune cell expansion rates in VGRID
T	=	temperature
U	=	streamwise velocity
U_C	=	crossflow velocity
U_e	=	boundary-layer edge velocity
U_∞	=	freestream velocity
X, x	=	chordwise coordinate
Y, y	=	spanwise coordinate
Z, z	=	vertical coordinate
α	=	angle of attack
Δ_n	=	normal grid spacing height for the nth layer
δ_{01}	=	distance from wall where U_C reduces to $0.1\lvert U_{C\ \max}\rvert$
δ_{99}	=	boundary-layer thickness (distance from wall to 99% of boundary-layer edge velocity)
η	=	distance normal to the wall (in meters)
λ	=	spanwise wavelength
ν	=	kinematic viscosity
ν_e	=	kinematic viscosity at the boundary-layer edge
σ	=	growth rate of disturbance

Presented as Paper 2012-2690 at the 42nd AIAA Fluid Dynamics Conference and Exhibit, New Orleans, LA, 25–28 June 2012; received 25 August 2013; revision received 16 December 2013; accepted for publication 27 February 2014; published online 16 June 2014.

*Research Scientist; Corvid Technologies, Mooresville, North Carolina 28117; wei.liao@corvidtec.com. Senior Member AIAA.

†Senior Aerodynamicist, Computational AeroSciences Branch; m.r.malik@nasa.gov. Fellow AIAA.

‡Aerospace Technologist, Computational AeroSciences Branch; e.lee-rausch@nasa.gov. Senior Member AIAA.

§Aerospace Technologist, Computational AeroSciences Branch; fei.li@nasa.gov.

¶Aerospace Technologist, Computational AeroSciences Branch; eric.j.nielsen@nasa.gov. Senior Member AIAA.

**Aerospace Technologist, Computational AeroSciences Branch; pieter.g.buning@nasa.gov. Associate Fellow AIAA.

††Aerospace Technologist, Computational AeroSciences Branch; m.m.choudhari@nasa.gov. Associate Fellow AIAA.

‡‡Aerospace Technologist, Computational AeroSciences Branch; chau-lyan.chang@nasa.gov. Senior Member AIAA.

I. Introduction

THE reduction of aerodynamic drag on flight vehicles continues to be a crucial issue because of the stringent energy efficiency requirements of today. The skin-friction drag is an important drag component and can make up to 50% of the overall vehicle drag. Therefore, a natural laminar flow (NLF) over an aircraft configuration is desirable because of the lower skin friction associated with it, as compared with turbulent flows. In situations in which a natural laminar flow is unattainable, laminar-flow control (LFC) may be employed to maximize the region of laminar flow. Affordable analysis methods that adequately account for transition from laminar to turbulent flows are critical for a viable laminar-flow technology and should be a part of the design process for NLF and LFC applications. The direct numerical simulations approach to resolve the boundary-layer instability scales in the laminar-turbulent transition process is prohibitively expensive because of the very fine computational grid required. LASTRAC [1–3] is a stability analysis code that is widely used to predict transition in practical applications.

In recent years, adjoint-based design optimization methodology has been developed and implemented in several large-scale computational fluid dynamics (CFD) codes. FUN3D [4–9], an unstructured CFD code developed at NASA Langley Research Center, provides extensive adjoint-based capabilities for design optimization for many

design parameters. An ultimate long-term goal of the present research is to develop an adjoint formulation for LASTRAC and integrate it with the adjoined-based capabilities of FUN3D to enable design optimization that maximizes the laminar-flow regions. As a stepping stone to that capability, a short-term goal would be to analyze aerodynamic flows with various stability analysis codes, identify flow characteristics critical for delaying transition, and include these characteristics in the objective function optimized by the existing adjoint-based method.

The first step toward the short-term goal is the extraction of accurate boundary-layer mean flows required for stability analysis. The boundary-layer mean flows can be obtained by a variety of methods, including direct computations using boundary-layer codes or extractions from Navier–Stokes solutions. Boundary-layer methods based on two-dimensional (2-D), quasi-three-dimensional (3-D), or conical approximation are both simple and efficient. However, their use in the context of strong 3-D flows, such as those over a finite-span wing glove, must be validated in comparison with higher-fidelity methods, such as a full Navier–Stokes solution for the laminar basic state. A possible alternative to the Navier–Stokes approach is the 3-D boundary-layer method, which will not be discussed in this paper.

As a first step, a procedure was developed to extract "stability quality" mean flows from flow solutions on unstructured tetrahedral and mixed-element grids, for which extensive validations were performed against mean flows extracted from structured-grid solutions ranging from a simple flat-plate flow to an infinite swept wing flow to a realistic flow configuration of a composite glove on the wing of a Gulfstream III (G-III) aircraft. Although the extraction procedure was tested on mean flows in which crossflow instability modes dominated, the use of this procedure is not limited to just these types of flows.

NASA's Environmentally Responsible Aviation Project selected a modified Gulfstream III aircraft fitted with a composite glove on one of its wings to evaluate a certain laminar-flow control concept for potential applications on transport aircraft [10,11]. A wing glove with NLF characteristics was designed through collaborative research between Texas A&M University and NASA Dryden Flight Research Center [12]. Figure 1 shows the glove as installed on the G-III aircraft wing. The G-III glove is thus a perfect test case for demonstrating the capability of the extraction procedure for realistic applications. FUN3D had been used earlier for 3-D CFD simulations of the G-III aircraft [11]. Stability analysis of the mean flows produced by boundary-layer codes, which used C_p obtained from the FUN3D solution as the boundary-layer edge condition, had also been conducted to provide some insight into the glove design [11]. In the current study, the stability analysis results based on the mean flows directly extracted from FUN3D solutions were compared to those based on other well-established codes, such as CFL3D [13,14] and OVERFLOW [15,16]. CFL3D had been extensively used for a number of laminar-flow applications associated with stability analysis [17–19], whereas the use of OVERFLOW had not been reported for this purpose. Because of its capability of handling complex aerodynamic configurations, OVERFLOW was used here to perform computations for the full G-III aircraft case, and the results were compared with FUN3D results for cross validation.

The rest of the paper is structured as follows: an overview of the computational tools is given in Sec. II, followed by a presentation of results and discussions in Sec. III. Finally, conclusions are drawn in Sec. IV.

II. Computational Tools

A general stability analysis procedure involves the following steps. First, flow solutions are obtained by a CFD solver. Then mean boundary-layer flow profiles can be obtained from the flow solutions by either of two means:

1) With the boundary layer well resolved by a Navier–Stokes solver, mean flow profiles may be extracted directly from computed laminar solutions.

2) The surface pressure distribution from the CFD solution is imposed as the edge conditions for a selected boundary-layer code to generate mean flow quantities.

Finally, with the obtained boundary-layer mean flows as a basis, stability analysis codes can be used to predict the linear and/or nonlinear development of instability modes. In this work, different tools or approaches may be used for cross-validation purposes at each step. The tools or approaches used here are briefly introduced next.

A. Numerical Tools for Flow Computations

1. *FUN3D: Unstructured-Grid Flow Solver*

FUN3D [4–9] is a suite of computational fluid dynamics codes, developed at NASA Langley Research Center, based on fully unstructured grids for flow analysis, adjoint-based design optimization, error estimation, and objective-based adaptive mesh refinement. FUN3D solves the Reynolds-averaged Navier–Stokes (RANS) equations using a node-centered second-order upwind implicit scheme. FUN3D can solve the equations on mixed-element grids, including tetrahedra, pyramids, prisms, and hexahedra. At control volume interfaces, the inviscid fluxes are computed using an approximate Riemann solver based on the values on either side of the interface. Several convective flux schemes are available in FUN3D. The most common scheme for subsonic and transonic flows is Roe's flux difference splitting [20], which is used in the current study.

FUN3D has an adjoint-based optimization module providing a very efficient design capability for complex aerodynamic configurations. The current study is the first step to couple the flow analysis and adjoint design capability of FUN3D with the NASA stability and transition prediction tool, LASTRAC, for NLF or LFC wing design.

2. *VGRID: Unstructured-Grid Generation*

The unstructured-grid tool VGRID [21], based on the advancing front method (AFM) and the advancing layers method (ALM), is employed to generate tetrahedral grids in the current study. The generation of a viscous grid is divided into three main steps: 1) generation of triangular surface grid by the ALM and/or AFM,

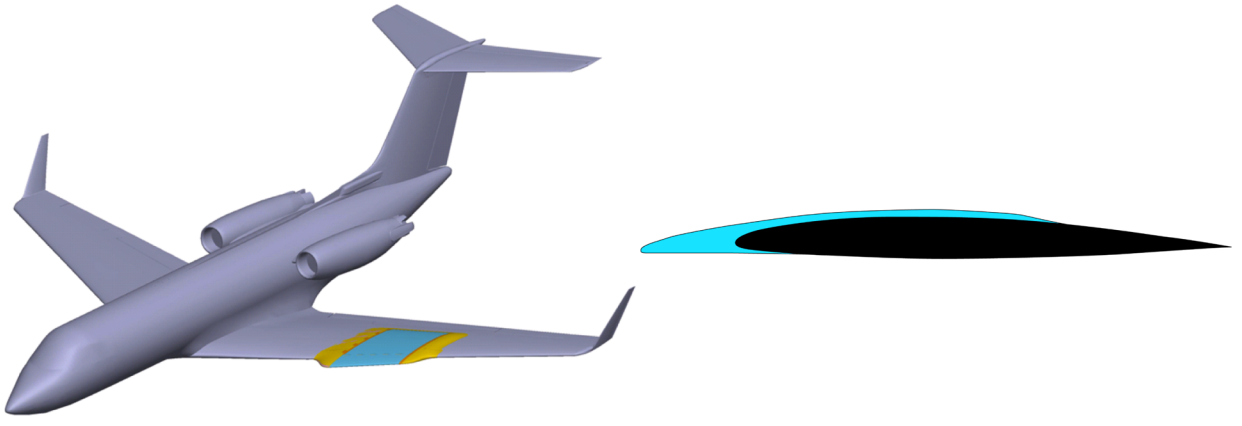

Fig. 1 G-III aircraft with a composite glove (left) and the midspan cross section of the wing glove (right).

2) generation of thin tetrahedral cells in the boundary layer by the ALM, and 3) generation of regular (inviscid) tetrahedral grid outside the boundary layer by the AFM. VGRID uses the following formula to establish the normal spacing for the nth layer in the advancing layers [21]:

$$\Delta_n = \Delta_1[1 + r_1(1 + r_2)^{n-1}]^{n-1} \tag{1}$$

where Δ_1 is the normal spacing of the first layer; r_1 is a geometric stretching rate; and r_2 is a modifier to r_1, which can be used to tune the cell expansion rate of viscous grid layers. Variable stretching ratios are allowed to use a set of smaller stretching ratios in the area of interest while using larger ratios elsewhere.

3. CFL3D and OVERFLOW: Structured-Grid Flow Solvers

CFL3D [13,14] is a well-known three-dimensional structured-grid flow solver developed from the 1980s at NASA Langley Research Center. CFL3D solves the time-dependent conservation law form of the RANS equations using a semidiscrete finite volume approach with upwind biasing of the convective and pressure terms and central differencing of the shear stress and heat transfer terms. In the current study, Roe's flux scheme [20] is chosen for flow analysis. One of the code's many strengths is the diversity of available turbulence models. CFL3D can handle one-to-one multiblock grids, patched grids, and overset grids as well.

OVERFLOW [15,16] is a RANS solver developed by NASA for structured grids, based on single-block grids or overset (structured) grid systems. When solving the flow equations, the convective term discretization options include central differencing with Jameson et al.'s artificial dissipation scheme [22] and Roe's flux scheme [20]. Grid sequencing and multigrid are implemented to accelerate convergence coupled with overset grid techniques. OVERFLOW is used to compute the full G-III aircraft case, with Roe's scheme in the grid block over the wing and the artificial dissipation scheme in the other blocks for better computational efficiency.

CFL3D and OVERFLOW are used in the present study for validation purposes.

B. Stability Analysis Tools

Based on the boundary-layer mean flow profiles obtained, LASTRAC [1,2] can be used to predict linear and/or nonlinear development of instability modes. The analysis can be conducted for both crossflow and Tollmien–Schlichting (TS) waves with three approaches: 1) linear (parallel) stability theory (LST); 2) linear parabolized stability equations; and 3) nonlinear parabolized stability equations. Stability calculations and N-factor correlations can be performed for both 2-D/axisymmetric [1] and general 3-D configurations [2].

The 3-D stability analysis module within LASTRAC is based on boundary-layer profiles at each point of a structured-grid surface mesh. In the present work, mean flows are extracted directly from Navier–Stokes solutions and fed to LASTRAC for 3-D analysis. There are multiple ways in which disturbance evolution in 3-D boundary layers can be computed by LASTRAC [2]. In this study, 3-D stability analysis is performed by marching along a path that is aligned with inviscid streamlines. In contrast, 2-D stability analysis using LASTRAC is usually based on mean flow profiles along a streamwise cut, which can be obtained by either 2-D/quasi-3-D boundary-layer codes or the extraction from Navier–Stokes solutions.

Another code, eMalik [23], a stability analysis code based on linear stability theory for 2-D or axisymmetric compressible wall-bounded flows, is also used for validation purposes in selected cases when necessary.

C. Boundary-Layer Codes for Boundary-Layer Profiles

Mean flow profiles for stability analysis can be generated via boundary-layer codes, using edge conditions based on the surface pressure and edge temperature from CFD computations or experiments. Here two boundary-layer codes were used for this purpose. WINGBL2 is a boundary-layer solver developed by Pruett and Streett [24] for an infinite swept wing. It uses spectral discretization in the surface normal direction and second-order backward difference along the marching direction. Because of the infinite-span approximation made in WINGBL2, only mean flow profiles with no spanwise variation in flow parameters can be produced. On the other hand, the BLSTA code can solve either 2-D, axisymmetric, or quasi-3-D laminar boundary-layer equations [25], and therefore can be used for infinite swept wings, sweptback, or forward tapered wings with a spanwise conical flow assumption, and even sweptback delta (low aspect ratio) wings with a streamwise conical flow assumption. It is based on second-order finite difference discretizations in both surface normal and marching directions.

D. Direct Extraction of Boundary-Layer Profiles from Navier–Stokes Solutions

Besides resorting to boundary-layer codes, one can extract boundary-layer profiles directly from laminar solutions computed by a Navier–Stokes solver. While the capability of dealing with unstructured meshes has been developed, this option is not fully functional; therefore, LASTRAC currently works only with structured mesh topologies. Boundary-layer mean flow profiles may be directly taken from the flowfields obtained by structured-grid flow solvers like CFL3D and OVERFLOW, but interpolation is needed for the solutions obtained from the unstructured flow solver FUN3D. As a result, an extraction procedure has been developed to construct an appropriate boundary-layer grid that is orthogonal and clustered near the wall boundary to provide a suitably dense basic state definition for the purpose of stability analysis.

The grid used for stability analysis begins from a leading edge, which is automatically detected using an iterative binary search procedure. The detected leading edge forms one edge of a 2-D planar structured grid. By specifying the domain extent in the streamwise and spanwise directions, users can thus define this planar grid completely. Then, FUN3D projects the 2-D grid onto the wing surfaces to obtain seed points. Profile points are then distributed along the wall-normal vectors computed at each seed point using clustering parameters specified by the user. The profile extent in the normal direction is determined by the boundary-layer thickness, which can be estimated by [26]

$$\delta_{99}(x) = 5\sqrt{\frac{\nu x}{U_\infty}} \tag{2}$$

where ν is the kinematic viscosity, x is the streamwise surface distance downstream from the start of the boundary layer, and U_∞ is the freestream velocity. The outer edge of the stability grid is determined as a fixed multiple of the boundary-layer thickness estimated by Eq. (2). The constant in Eq. (2) can be adjusted to account for pressure gradient effect if needed. Users can define the number of spanwise locations based on resolution requirements. A stretching function is implemented to cluster the stability grid in each spanwise plane at areas near the leading edge and the wall surface. Figure 2 illustrates a sample stability grid established by the current projection procedure.

FUN3D identifies the unstructured-grid element containing each profile point on the stability grid. The flow variables on the newly constructed grid are then interpolated from their values at the surrounding grid points in the element. FUN3D can solve the equations on mixed-element grids, including tetrahedra, pyramids, prisms, and hexahedra. However, interpolation is always based on tetrahedral cells, as this is the only option currently implemented in the code. To interpolate at a particular point, the first step is to determine which mesh element the point is in. If this element is not tetrahedral, this element will be temporarily subdivided into tetrahedra. A hexahedron, prism, and pyramid can be subdivided into six, three, and two tetrahedra, respectively. Once the tetrahedron containing the interpolation point is identified through a search procedure, quantities are computed with first-order accuracy as a weighted sum of the values at the vertices of that tetrahedron based on the barycentric coordinates of the interpolation point.

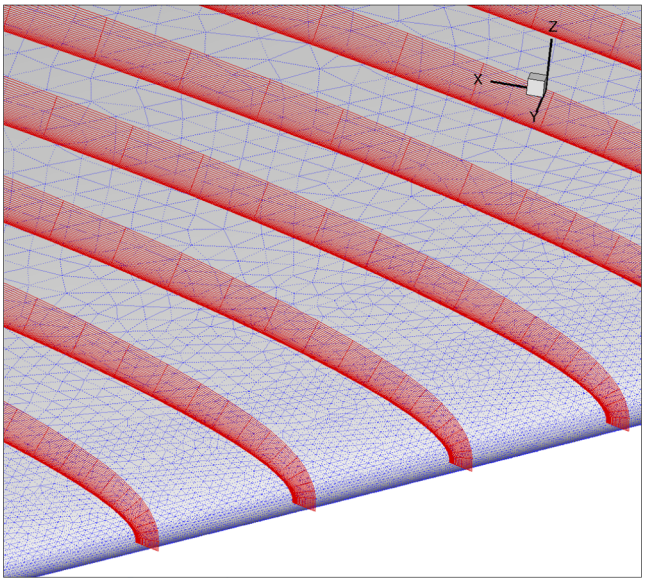

Fig. 2 Sample stability grid established by the extraction procedure implemented for an unstructured-grid flow solver.

The aforementioned extraction process has been parallelized and integrated within the FUN3D solver. With this procedure, mean flow profiles for boundary-layer stability analysis can be derived from the Navier–Stokes solutions immediately after a CFD computation is done. The profiles extracted from the unstructured Navier–Stokes solutions are output as PLOT3D grid and solution files.

E. Laminar Region Specification

Mean flows for stability analysis must be based on laminar-flow solutions. Therefore, whenever one is concerned with the instability of the laminar boundary layer in selected regions of the wing, laminar flow must be imposed in the corresponding zones, whereas turbulence models are used for all the other regions. The CFD solvers used here have recently incorporated turbulence models based on a built-in transition procedure as described in Rumsey and Lee-Rausch [14] However, laminar-flow regions were manually specified in the present study.

A laminar-flow specification approach has been incorporated into FUN3D, by which multiple laminar-flow regions in the flowfield can be manually specified based on the flow physics and numerical requirements. In this approach, arbitrary line sections are introduced to define different shapes of laminar zones and specify multiple transition locations in the flow field. As a result, "laminar" and "turbulent" regions are defined, respectively, upstream and downstream of the transition locations. The approach implemented in FUN3D, CFL3D, and OVERFLOW to specify transition locations is based on the idea of turning off the turbulent production terms in the laminar regions of the grid [27]. The flow usually remains laminar inside the specified regions as a result. Full turbulence model equations are used everywhere, although their turbulence production terms are turned off in the specified laminar regions. Turning off the production term may not prevent turbulence from convecting or diffusing into laminar regions near the transition boundaries. So, the specified laminar regions should usually be larger than the areas of actual interest. Most importantly, the values of turbulence viscosity should be checked to ensure laminar flows in the areas of interest.

Since both CFL3D and OVERFLOW are structured-grid flow solvers, the laminar region specification in them is based on (i, j, k) grid point indices in a grid block instead of (x, y, z) coordinates used in FUN3D. As a result, when these codes are used to compute the same case, the laminar-flow regions specified may have slight differences. Note that, in the current study, the Spalart–Allmaras [28] model is always chosen for turbulence computations although a variety of turbulence models are available in all three codes.

III. Results and Discussions

This section presents the results of computations aimed at validating the mean flow extraction procedure. The first two cases involve relatively simple flow configurations of a flat plate and an infinite swept wing, respectively. Then, the more realistic case of a simplified G-III wing glove assembly is examined, in which the fuselage, engine, and winglet were removed from the full aircraft configuration. Finally, computations of the full G-III aircraft including the fuselage, engine, and winglet are carried out.

A. Flat Plate

The first case to be examined is the flow over a semi-infinite flat plate for which a similarity solution exists. The freestream Mach number and unit Reynolds number were chosen to be 0.5 and 1×10^6 per meter, respectively. The FUN3D solver was used to compute the laminar flowfield in a computational domain that extended to 1 m upstream and 3 m downstream of the flat-plate leading edge, with the spanwise width of 1 m and the upper boundary fixed at 0.06 m above the plate (i.e., approximately six times the boundary-layer thickness at the end of the computational domain). A very fine unstructured grid with pure tetrahedron cells containing 14.4 million nodes was generated using VGRID [21] to resolve the boundary layer. The grid spacing was determined by Eq. (1) with $r_1 = 0.028$, $r_2 = 0$, and $\Delta_1 = 6 \times 10^{-6}$ m. Figure 3 shows the grid distribution on the wall surface (X-Y) and at the midspan cut normal to the wall (X-Z). For validation purposes, CFL3D computations were conducted using two different structured grids with the resolutions of 257×193 and 513×385, respectively.

The extraction procedure was employed to obtain boundary-layer profiles from the FUN3D solution. Comparisons of the streamwise velocity profiles with the CFL3D solution and the Blasius similarity solution, along with the first and second derivatives of the mean velocity profiles, are shown in Fig. 4. For the velocity and its first derivative, there is excellent agreement among the three solutions. In contrast, the second derivative from the FUN3D solution displayed significant oscillations, which is not surprising because a first-order linear interpolation was used to extract boundary-layer profiles from the FUN3D solution. After smoothing via iteratively solving the Laplace's equation [29], very good agreement is found among the three solutions.

Next, the LASTRAC code was used to perform stability computations of TS instability waves based on FUN3D and CFL3D solutions and the eMalik [23] code was used to analyze the stability of the self-similar mean flow. Figure 5 shows the instability growth rates at two spatial locations, $x = 0.945577$ m and $x = 1.96839$ m. The results from different computations are in good agreement. It is important to note that the stability analysis for FUN3D was based on its original boundary-layer profiles without smoothing. In this case, the oscillations in the second derivative profiles had no perceptible influence on the linear stability results because the second derivative terms only appear in the viscous part of the compressible linear stability equations:

1) Viscous terms are $1/Re$ of the inviscid terms.

2) The mean flow second derivative further multiplies perturbation to dynamic viscosity, which is a small term. Such oscillations would have generated completely erroneous results for the solution of an incompressible Orr–Sommerfeld equation where second derivative terms appear from the inviscid part of the Navier–Stokes equations.

Numerical tests also revealed that, while the residual of the numerical solution needs to converge by only three to four orders of magnitude for the computation of aerodynamic forces to engineering accuracy, it must converge by six to seven orders of magnitude if the solution is intended for stability analysis.

B. Infinite Swept Wing

The second test case is an infinite-span wing with a sweep angle of 34.58 deg and an angle of attack equal to 2.7 deg. The cross section has the same shape as that of the G-III wing glove shown in the right plot of Fig. 1. The freestream Mach number and the chord Reynolds number are, respectively, 0.75 and 22×10^6. Both CFL3D and

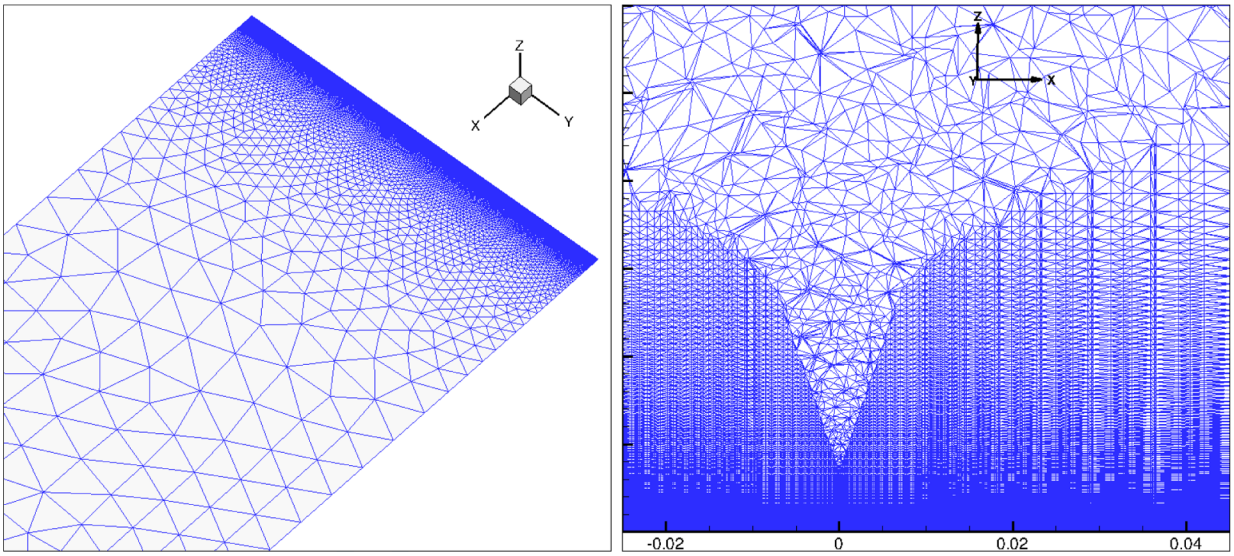

Fig. 3 Unstructured grid in *X*-*Y* plane (left) and *X*-*Z* plane (right) for the flat plate.

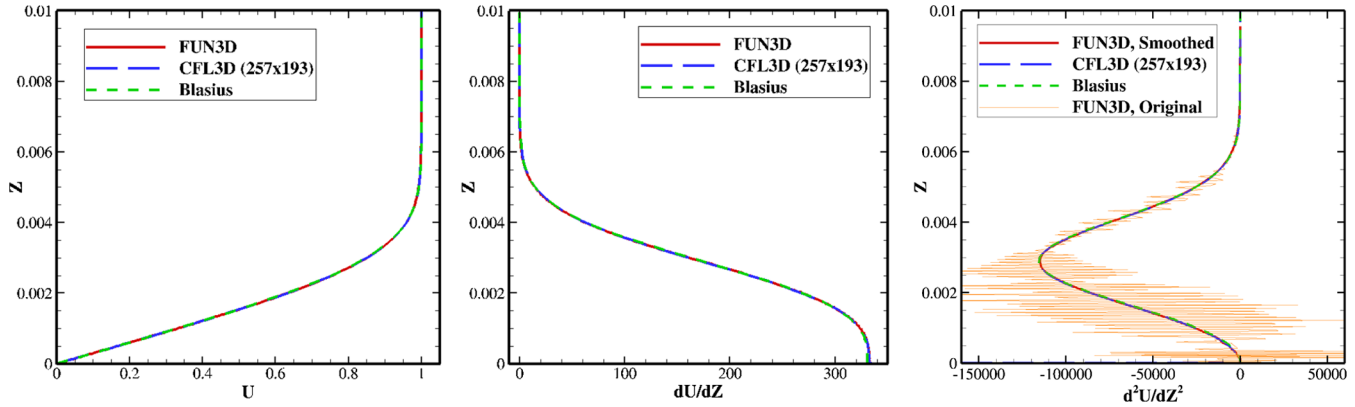

Fig. 4 Profiles of the velocity and its first and second derivatives over the flat plate.

FUN3D solvers were used for mean flow computations. The structured grid for the CFL3D computation had a grid size of 737 × 5 × 257 in streamwise, spanwise, and wall-normal directions, respectively, with the outer boundary extending in all directions to distances of approximately 50 times the chord length away from the wing surface. This structured grid was then converted to an unstructured grid for FUN3D computations. The extraction procedure was used to obtain the mean flow from the solutions based on pure tetrahedral cells. For both computations, the periodic boundary conditions were used in the spanwise direction.

The surface pressure coefficient C_p was extracted from the FUN3D solution and compared in Fig. 6a with that from the CFL3D

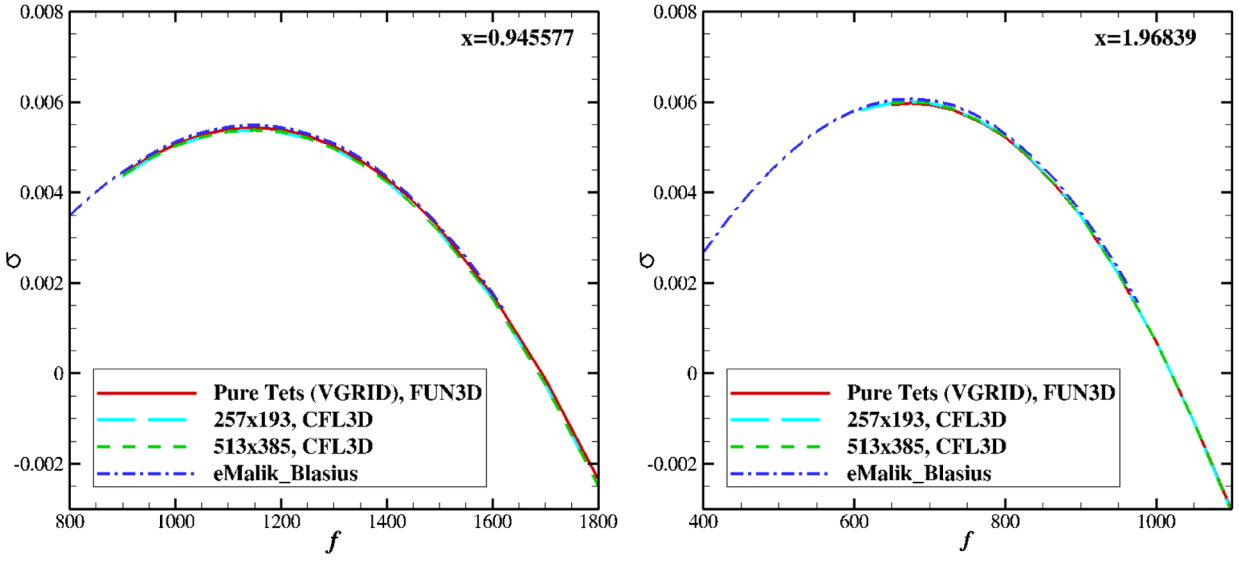

Fig. 5 Growth rate versus disturbance frequency (in hertz) at two spatial locations over flat plate. Here Tets stands for Tetrahedrons.

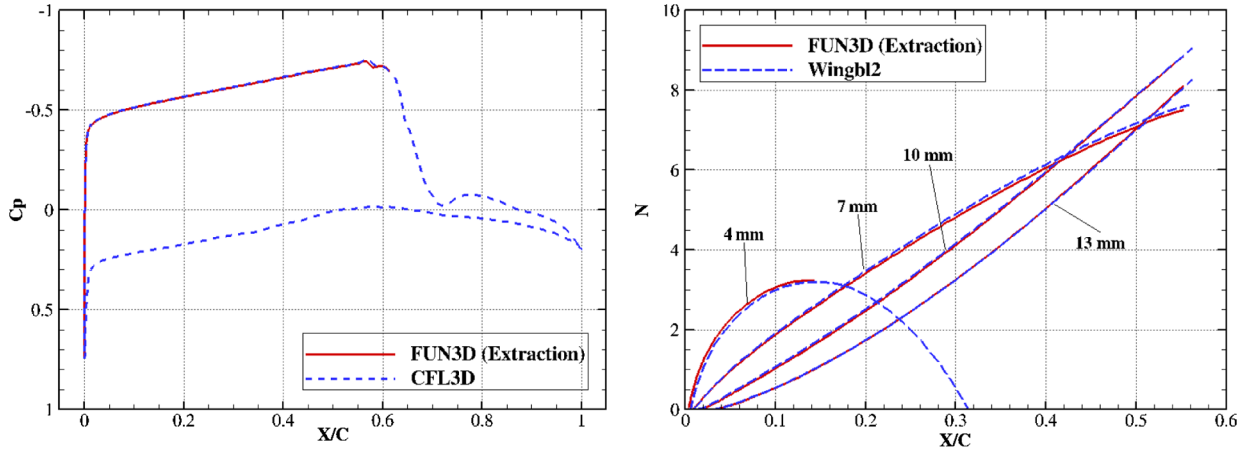

Fig. 6 Representations of a) C_p distributions from FUN3D through the extraction procedure and CFL3D (left) b) stationary crossflow LST N factors based on the mean flows from FUN3D and WINGBL2.

solution. The agreement is excellent. The extracted surface pressure coefficient distribution was then used for the generation of a mean flow by the WINGBL2 boundary-layer code. The mean flows extracted from the FUN3D solution and those generated by WINGBL2 boundary-layer solution were used for linear stability analysis by LASTRAC. Figure 6b shows the N factors for stationary crossflow instability modes with the spanwise wavelengths of 4, 7, 10, and 13 mm. The agreement between N factors based on the mean flows of different origins is quite good.

In this case, the effect of the interpolation in the extraction procedure on the velocity profiles used for stability analysis was also investigated. For this purpose, the boundary-layer profiles were obtained by two approaches from the FUN3D solution on the unstructured grid. The first approach was based on the extraction procedure involving an interpolation, whereas the other approach directly converted the unstructured solution to the structured one without interpolation. The temperature, the streamwise and crossflow velocity profiles obtained using these two approaches, and their first and second derivatives are compared in Fig. 7. The agreement is excellent between two approaches for mean flow variables and their first derivatives. In contrast, significant oscillations were observed for the second derivatives, based on the extraction approach, whereas their counterparts, based on the direct conversion, were very smooth. After iterative smoothing of the interpolated mean flow profiles via Laplace's equation [29], very good agreement is seen between the two sets of profiles. This clearly shows that these oscillations are mostly, if not entirely, caused by the first-order linear interpolation employed in the extraction procedure. The oscillations can be eliminated by Laplacian smoothing and do not produce a noticeable change in the mean values of the profile. As noted for the flat-plate case before, the oscillations in the second derivative profiles do not have any perceptible influence on the stability results. This is not a general conclusion, and higher-order interpolations for profile extraction should be explored, but it is considered beyond the scope of this paper.

C. Gloved Wing Only

The validation tests carried out so far in Secs. III.A and III.B show that the extraction procedure works satisfactorily, at least for simple flow configurations. In this subsection, computations were performed for a simplified G-III wing-glove assembly with the fuselage, engine, and winglet removed from the full aircraft for computational expediency.

For this configuration, the glove leading-edge sweep angle was 34.58 deg, which is slightly larger than that of the wing itself. The freestream Mach number and the chord Reynolds number were, respectively, 0.75 and 24.2×10^6, with the ambient pressure and temperature chosen to be those at an altitude of 38,400 ft in the standard atmosphere. The wing-glove assembly had an angle of attack of 3.4 deg.

Two unstructured grids with mixed elements were generated using VGRID [21] for FUN3D viscous flow computations. These two grids contain approximately 68.9 and 46.6 million nodes, respectively. The mixed-element grids consisted of tetrahedra, pyramid, and prisms, where the prisms were generated by recombining the tetrahedral grid in the advancing layers. The finer grid consisted of 23.8 million tetrahedra, 128.4 million prisms, and 1.2 million pyramids, whereas the coarser grid had around 24.7 million tetrahedra, 83.7 million prisms, and 0.96 million pyramids. The grid spacing for both meshes was determined by Eq. (1) with $\Delta_1 = 1.4 \times 10^{-4}$ to ensure that $y^+ < 1$ everywhere. Since a uniform stretching ratio was used for satisfactory grid quality, the grid sizes became relatively large as a result. The stretching ratios were $r_1 = 0.0125$ and $r_2 = 0.01$ for the finer grid, and they were $r_1 = 0.03$ and $r_2 = 0.01$ for the coarser grid. The number of nodes inside the boundary layer at any fixed location was approximately 80 and 50, respectively, for the two grids.

A multiblock structured grid with a total number of 112 million points was also generated by GRIDGEN for CFL3D simulations. There were approximately 110 points inside the boundary layer at any location in the glove region. Figure 8 shows both the unstructured and structured surface meshes of the wing-glove assembly.

For FUN3D computations, the residual for the mass conservation was driven to decrease by seven orders of magnitude relative to the initial residual, and for the CFL3D computations, it was decreased by six orders of magnitude. Consistency in the solutions can be seen in the surface pressure coefficient contours shown in Fig. 9.

Since the present case was fully 3-D, the 3-D capability of LASTRAC was used for stability analysis. Two sets of mean flows over the glove region were respectively extracted from the coarser and finer FUN3D unstructured-grid solutions, and a third set was directly obtained from the CFL3D structured-grid solution. For both FUN3D mean flows, 61 spanwise stations were extracted over the spanwise width of the glove. Linear stability analysis was performed on each of the mean flows for stationary crossflow instability modes with spanwise wavelengths of 5, 7, 9, and 11 mm. The N factors based on the three mean flows along a streamline that starts from a point at the midsection of the glove near the leading edge are shown in Fig. 10 along with the streamline. The coincidence of the streamlines derived from the three different solutions is observed. The general agreement is good among the N factor curves. A useful conclusion from this exercise is that, even with only 50 points in the boundary-layer resolution, the results of the stability analysis are as good as those with much higher resolution in the wall normal direction.

In addition to streamwise and wall-normal resolutions, the spanwise resolution used to extract the mean flow could also affect the accuracy of stability analysis. Therefore, a new mean flow was extracted from the finer FUN3D solution with an increased spanwise resolution, i.e., the number of spanwise stations over the width of the glove was increased from 61 to 91. N factors for the same stationary crossflow instability modes are plotted in Fig. 11 based on the two

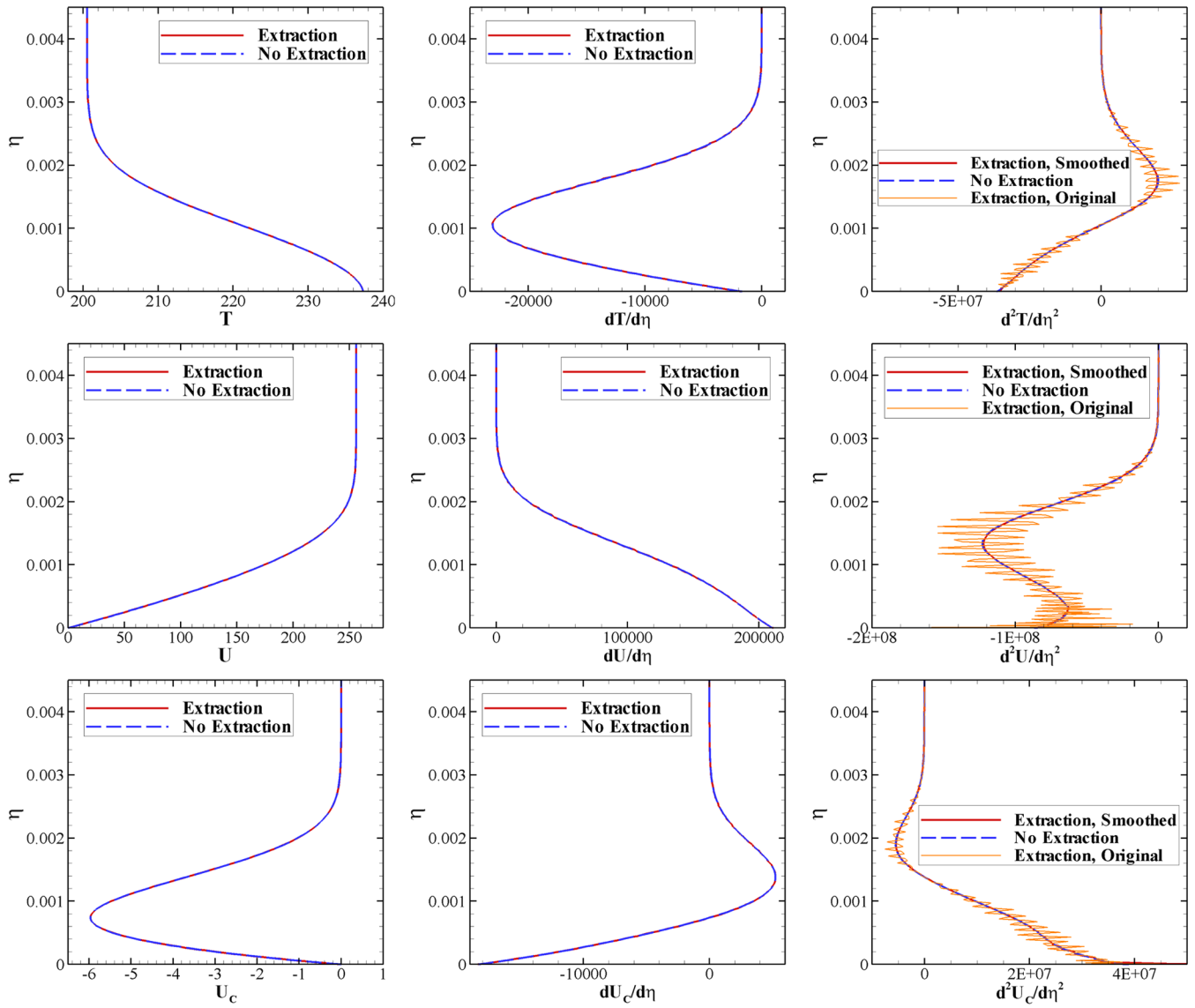

Fig. 7 Comparison for the temperature (in Kelvins), streamwise and crossflow velocities (in meters per second), as well as their first and second derivatives at $x/c = 0.294$ with and without interpolation.

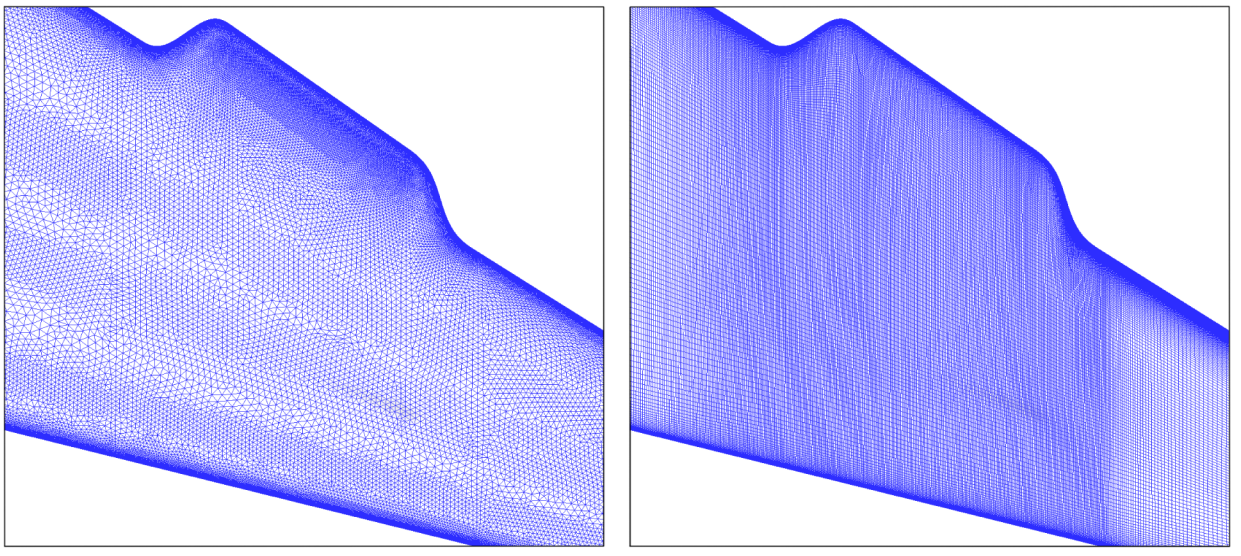

Fig. 8 Unstructured (left) and structured (right) grids used for FUN3D and CFL3D, respectively.

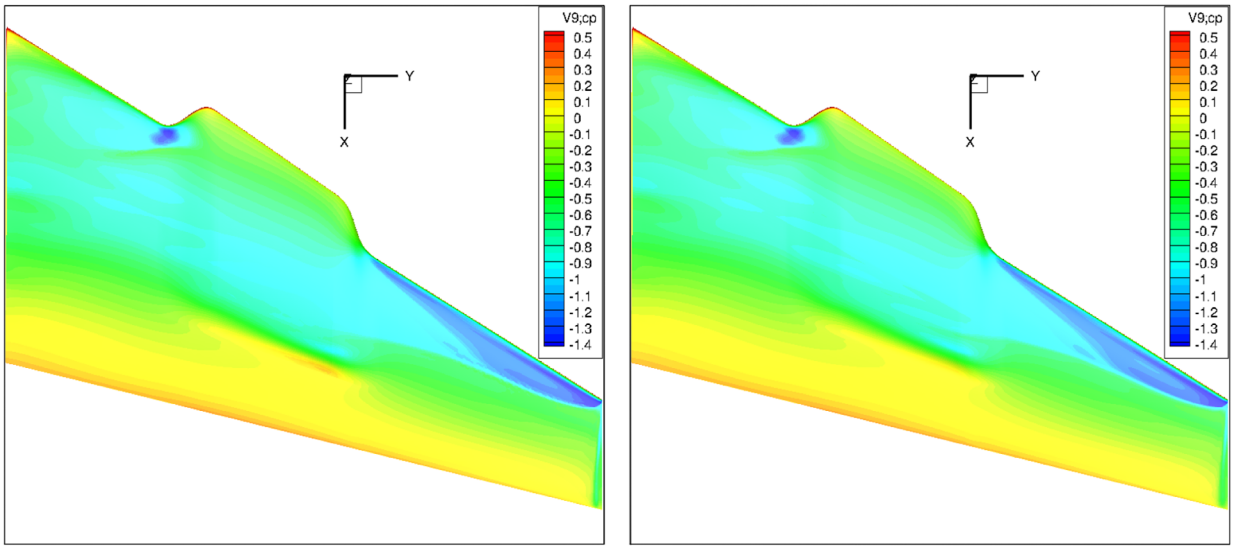

Fig. 9 C_p contours for FUN3D (left) and CFL3D (right).

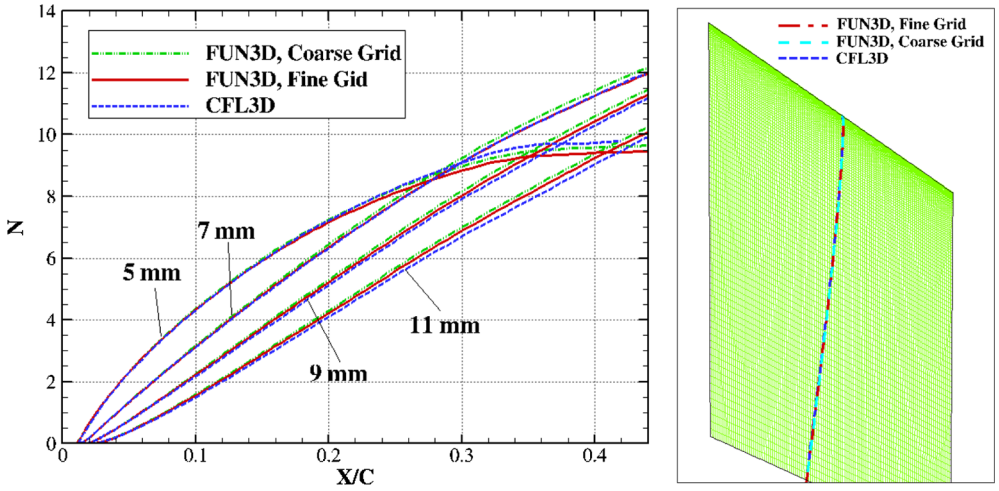

Fig. 10 3-D LST *N* factors based on the mean flows obtained from FUN3D and CFL3D solutions (left) and the corresponding streamlines along which stability analysis was conducted (right).

mean flows with different spanwise resolutions. The agreement is good, showing that 61 stations in the spanwise direction were sufficient for stability analysis with the instability modes computed herein.

D. Full G-III Aircraft with the Gloved Wing

In this section, computations over the full G-III aircraft configuration, including the fuselage, engine, and winglet, were performed. In this case, only one-half of the aircraft was gridded as flow symmetry was assumed along the centerline of the fuselage. Since the region of particular interest for this study was the midspan region of the wing, the tail was not simulated and some minor details of the engine nacelle geometry were ignored. The freestream flow conditions were exactly the same as those for the wing-glove-only case. Powered engine conditions as provided by H. Fletcher[§§] were used for the computation of the aircraft flowfield. A mixed-element unstructured grid was generated by VGRID [21] with a total of 25.7 million nodes. The near-wall mesh consisted of 38.8 million prismatic elements, the far-field mesh consisted of 34.5 million tetrahedron elements, and 0.48 million pyramids worked as transitional elements. Figure 12 depicts the unstructured surface grid generated for the full G-III aircraft. The unstructured and structured surface grids for the glove region are shown in Fig. 13, where $Y = 234$ in. signifies the distance from the center of the aircraft fuselage.

The grid spacing for the unstructured grid was determined by Eq. (1) with $r_1 = 0.03$ and $r_2 = 0.005$ in the glove region to ensure a

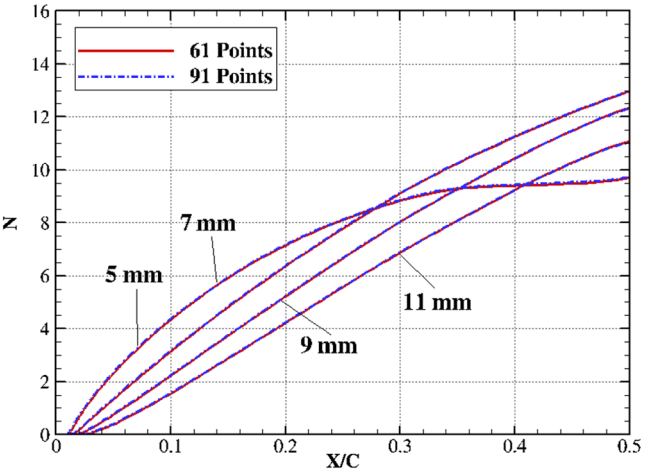

Fig. 11 Comparison of the 3-D LST *N* factors for four stationary crossflow modes (5, 7, 9, and 11 mm) by using 61 and 91 spanwise stations in the extraction procedure.

[§§]Private Communication with H. Fletcher, NASA Dryden Flight Research Center, Edwards, CA 2011.

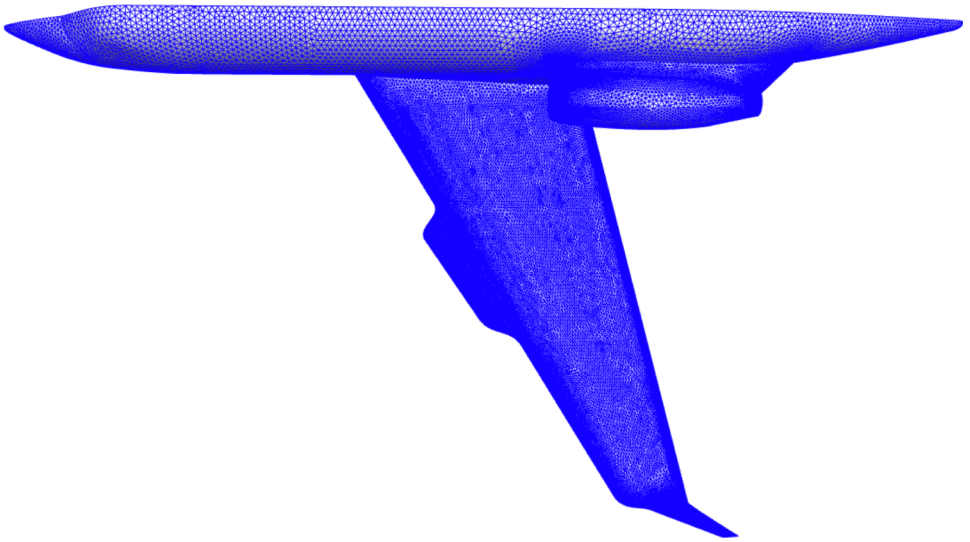

Fig. 12 Unstructured surface grid for the G-III aircraft.

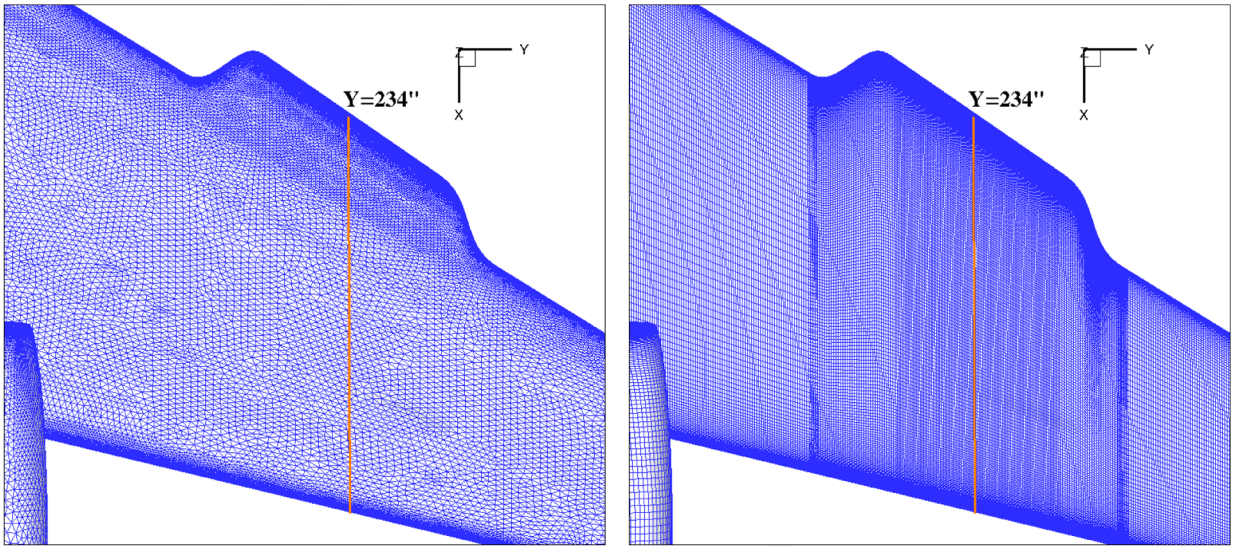

Fig. 13 Unstructured (left) and structured (right) grids on the surface of the G-III aircraft used for the FUN3D and OVERFLOW computations, respectively.

good resolution of approximately 50 points in the boundary layer, and $r_1 = 0.12$ and $r_2 = 0.02$ elsewhere to reduce the total grid size. $\Delta_1 = 1.4 \times 10^{-4}$ was used everywhere, as in Sec. III.C. The use of different stretching ratios in the glove region and beyond resulted in grid skewness and grid discontinuity, as evidenced in Figs. 14 and 15. The grid skewness also prevented further refinement of the boundary-layer mesh. Care was taken to assure that boundary-layer profiles for stability analysis were derived from the region without grid discontinuity (see Fig. 15b).

For validating the mean flow extracted from the FUN3D solution, OVERFLOW was used to perform computations on a structured overset grid, with the gloved wing, fuselage, and engine each residing in its own single block. There were 100–120 points across the boundary layer in the block over the glove region. The background Cartesian grid was generated automatically by OVERFLOW. The total number of points in the overset grid was 35.1 million. The right side of Fig. 13 shows the overset grid on the surface of the gloved wing. Figure 16 displays the overset grids before and after hole cutting at the midspan of the G-III glove.

The distribution of surface pressure (i.e., its gradient) is the most important factor dominating the crossflow development in 3-D boundary-layer flows. Figure 17 illustrates the pressure coefficient

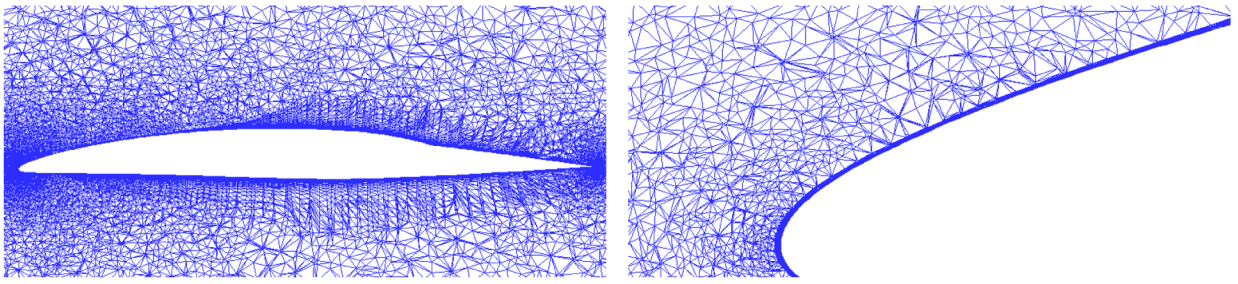

Fig. 14 Unstructured grid on the plane at the midspan ($Y = 234$ in.) of the G-III glove.

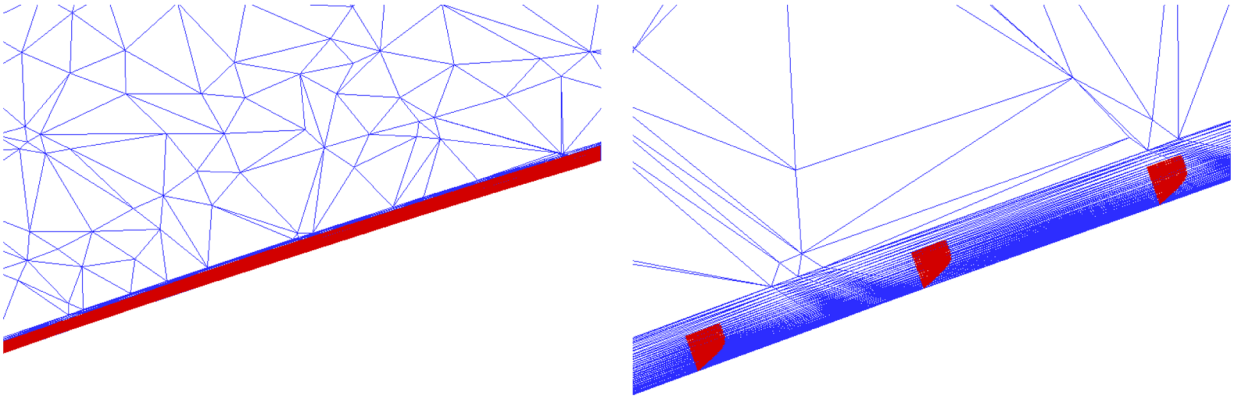

a) b)

Fig. 15 Representations of a) extent of stability grid in the wall normal direction and b) extracted mean flow profiles on the plane at the midspan of the G-III glove.

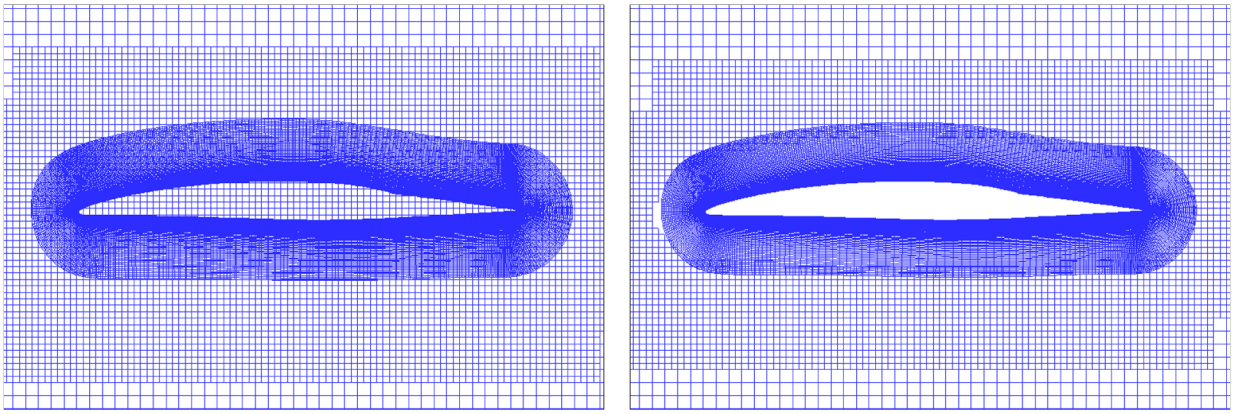

Fig. 16 Overset grids before (left) and after (right) hole cutting used for OVERFLOW computations at the midspan of the G-III glove.

contours computed by FUN3D and OVERFLOW over the gloved wing of the G-III aircraft. Good agreement is seen between these two solutions, except for minor differences near the inboard section of the glove. The solid lines in Fig. 17 show a streamwise cut that had been made at the midglove location of each solution. Figure 18 shows the plots of the corresponding pressure coefficient distributions along this cut, with excellent agreement observed between the FUN3D and OVERFLOW solutions. In these computations, turbulent flow was assumed everywhere except on the glove upstream of the shock. Laminar-flow computations were performed on the glove while RANS computations were performed elsewhere.

The crossflow Reynolds number R_{CF} is an important indicator of the strength of crossflow instability and is, therefore, most relevant for the purpose of validating the extraction procedure designed to construct mean flows for stability analysis. Figure 19 shows comparison of various mean flow parameters, including the crossflow Reynolds number R_{CF}, the streamwise Reynolds number Re_y, the dimensional (in meters per second) and nondimensional maximum crossflow velocities ($U_{C_{\max}}$ and $U_{C_{\max}}/U_e$), the crossflow length scale (δ_{01}, in meters), and the boundary-layer edge kinematic viscosity (ν_e, in squared meters per second) based on FUN3D and OVERFLOW solutions. The crossflow Reynolds numbers based on

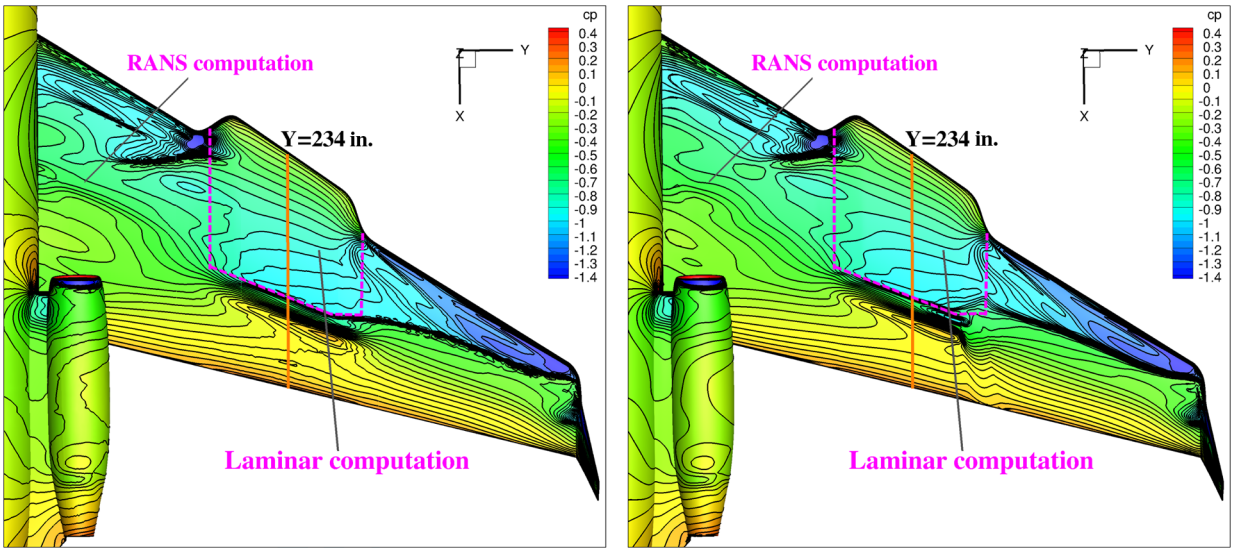

Fig. 17 C_p contours computed by FUN3D (left) and OVERFLOW (right) on the surface of G-III with the gloved wing.

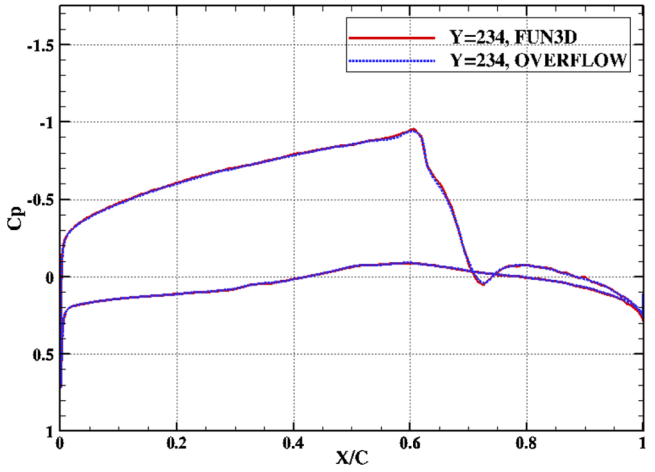

Fig. 18 Comparison of C_p distributions calculated by FUN3D and OVERFLOW along the midspan of the glove.

the two solutions along the same midspan cut are compared in the upper left corner of Fig. 19. Good agreement is observed upstream of the chordwise location $x/c = 0.4$, beyond which a rather significant difference began to appear. Also, nonsmoothness can be seen in R_{CF} for FUN3D. In contrast, there is an excellent agreement between the streamwise Reynolds numbers Re_y. Note that the mean flow quantities for FUN3D were obtained through interpolation in the extraction procedure, whereas those for OVERFLOW were obtained directly from the values at grid points without any interpolation, as the structured grid was designed to have a grid plane at the midspan of the glove. R_{CF} is a much more sensitive quantity than Re_y since R_{CF} is related to $U_{C_{\max}}$ and δ_{01}, both of which are very small quantities. Figure 19 shows that the magnitude of $U_{C_{\max}}$ is around 2–3% of U_e. δ_{01} is the distance from the wall where U_C reduces to $0.1|U_{C_{\max}}|$, which implies that δ_{01} is associated with a quantity that is one order of magnitude smaller than $U_{C_{\max}}$. From the plots for δ_{01} and $U_{C_{\max}}$, one can see a similar discrepancy between FUN3D and OVERFLOW as well as nonsmoothness in the curves based on the interpolated FUN3D profiles. Given that the crossflow Reynolds number is such a sensitive quantity and its computation based on Navier–Stokes solutions is subject to uncertainties associated with interpolation and determination of the boundary-layer edge, noted oscillations in R_{CF} are not surprising.

Figures 20 and 21 show the profiles in the wall-normal direction at two different locations, respectively, for both FUN3D and OVERFLOW solutions. The profiles of the streamwise and crossflow velocities are displayed in the figures along with the profiles of their first and second derivatives. Generally, there is good agreement between the solutions from FUN3D and OVERFLOW. Not surprisingly, large oscillations were observed again for the second derivative profiles from FUN3D, whereas the counterparts from OVERFLOW

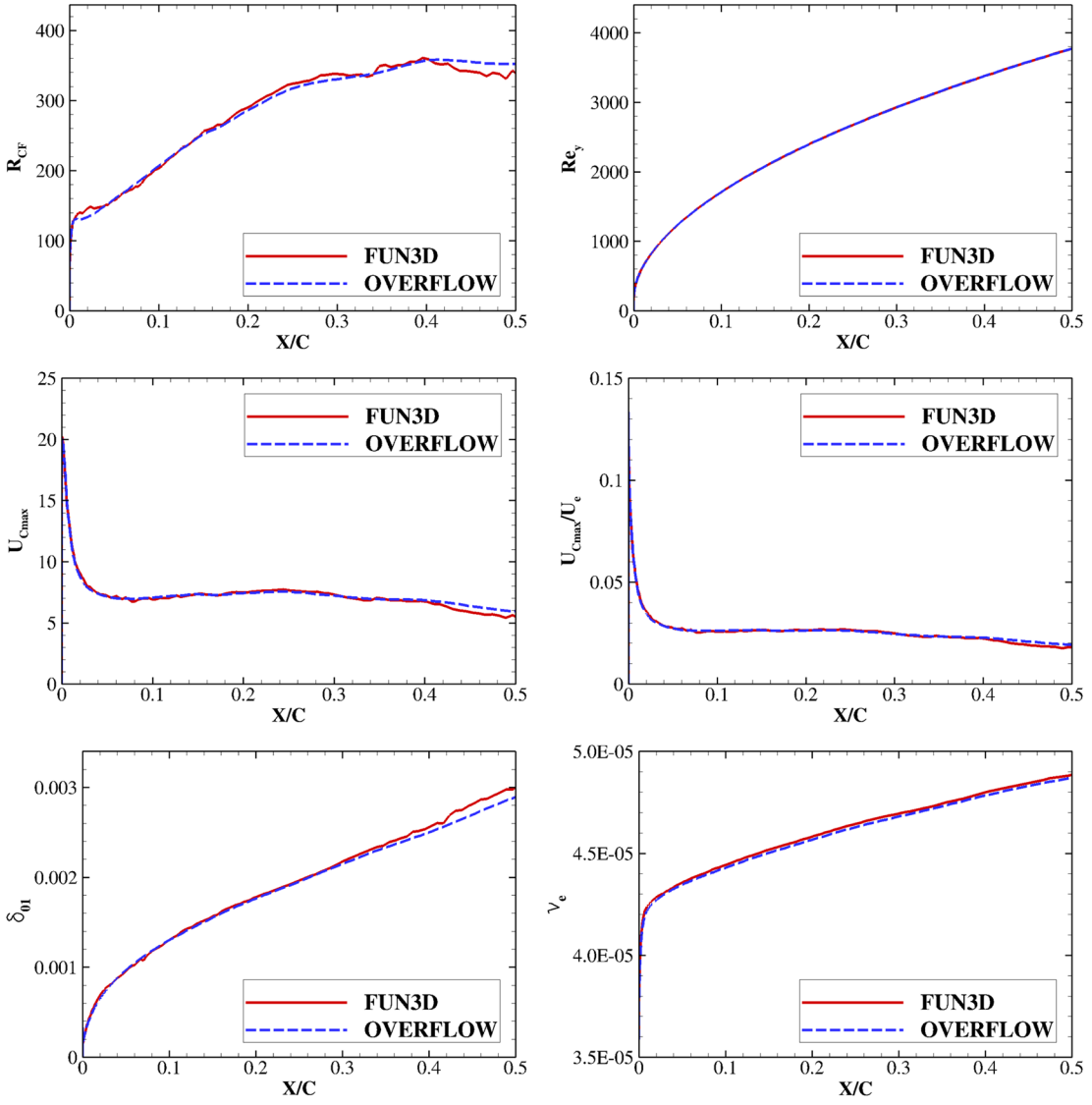

Fig. 19 Comparison of various mean flow parameters based on FUN3D and OVERFLOW solutions.

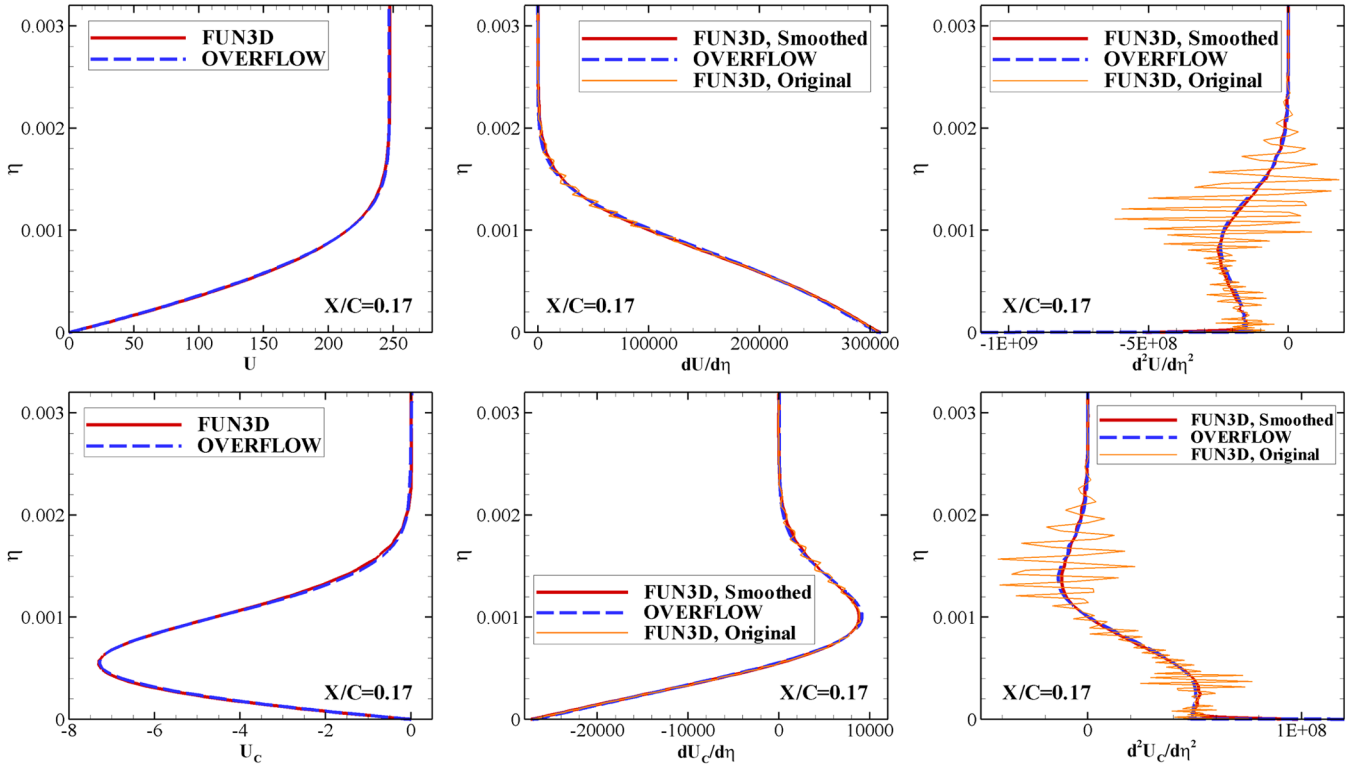

Fig. 20 Profiles of streamwise and crossflow velocities (in meters per second) and their first and second derivatives at $x/c = 0.17$ along the midspan of the glove.

were quite smooth. However, there were small oscillations in the profiles of first derivatives based on FUN3D solutions, which are displayed in the middle plots of both Figs. 20 and 21. Particularly, in the middle plot of Fig. 20, the lines show obvious zigzags in the range $0.001 < \eta < 0.002$. In contrast, such oscillations were not seen in the previous cases where the same interpolation procedure was used. These oscillations were likely from the FUN3D solutions themselves instead of from the linear interpolation. It could be improved by increasing the grid resolution on the glove surface and further enhancing the grid quality in the boundary layer. After smoothing again, the first and second derivatives match quite well with the OVERFLOW solutions.

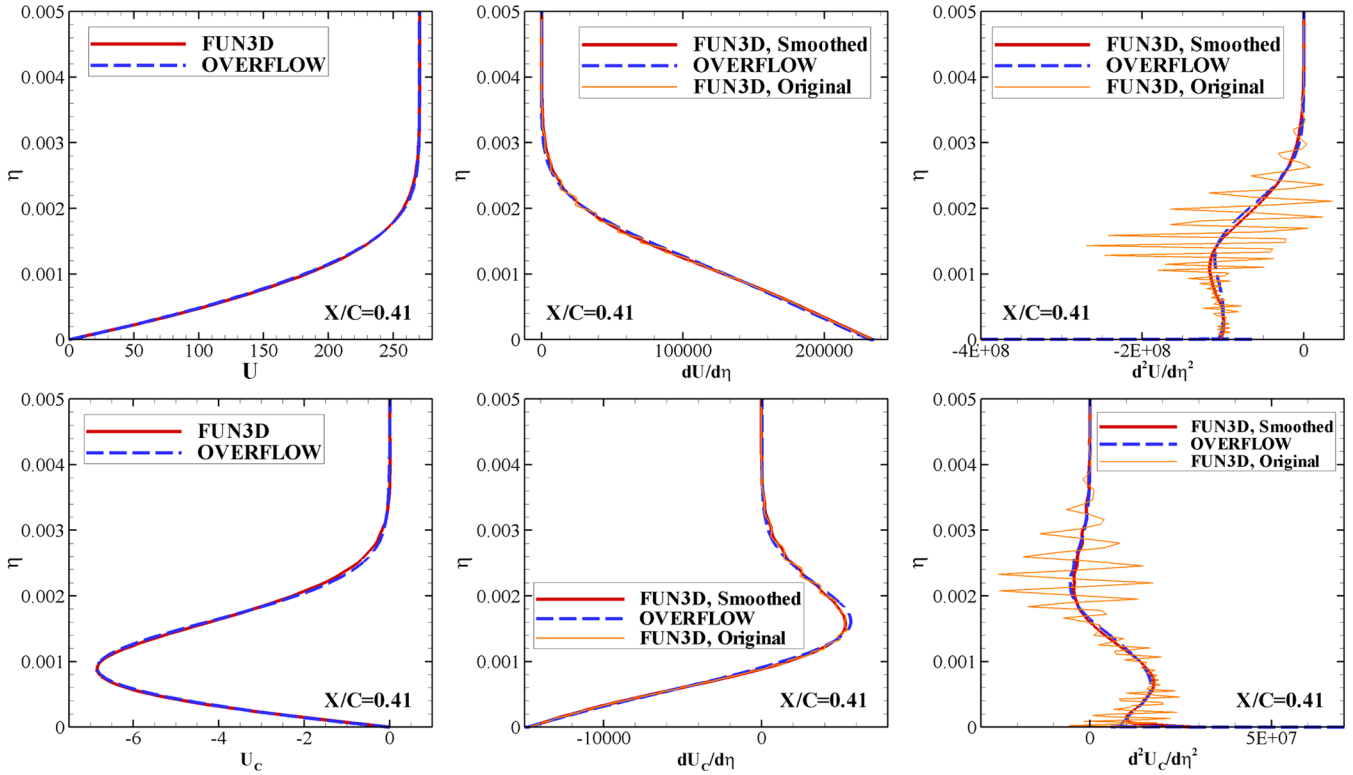

Fig. 21 Profiles of streamwise and crossflow velocity (in meters per second) and their first and second derivatives at $x/c = 0.41$ along the midspan of the glove.

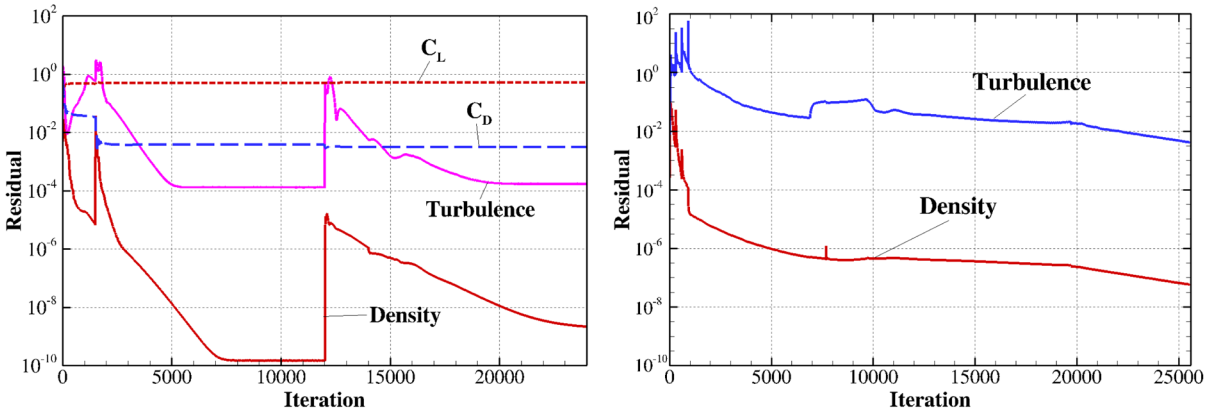

Fig. 22 Convergence history of FUN3D (left) and OVERFLOW (right) computations.

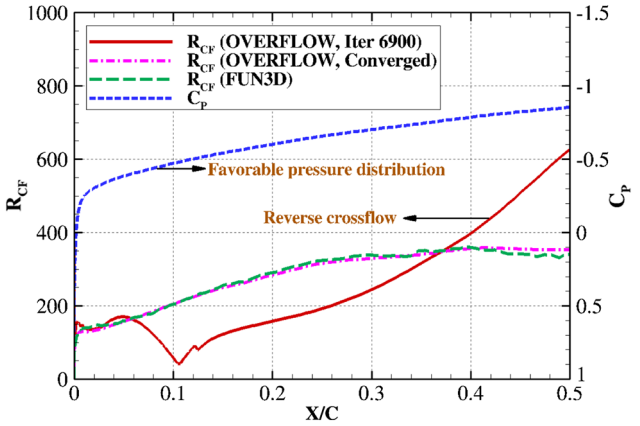

Fig. 23 Crossflow Reynolds numbers obtained by OVERFLOW on the midspan of the glove at the time steps of 6900 and 25,600.

Figure 22 displays the convergence history for both FUN3D and OVERFLOW computations. For the FUN3D computation, there were convergence issues when laminar flow was specified on the glove. Thus, a fully turbulent computation was performed first for initialization purposes. To further enhance the convergence, 1500 first-order iterations were performed before employing second-order spatial accuracy. The left plot of Fig. 22 shows that the flow residual in the FUN3D computation converged by seven orders of magnitude, whereas the turbulence residual converged by around four orders. In contrast, C_L and C_D converged in much fewer iterations. Also, it is worthwhile to mention that, in the OVERFLOW computations, crossflow components in the boundary layer took a very long time to converge. At time step 6900 with the residual dropped around six orders, an excellent agreement of C_p between OVERFLOW and FUN3D had already been achieved, which can be seen clearly from Fig. 18. As shown in Fig. 23, however, the crossflow distribution had not converged yet; in fact, crossflow changed sign at $x/c \approx 0.1$, which is obviously unphysical for a favorable pressure distribution. With computation continuing to time step 25,600, the residual dropped more than seven orders of magnitude. As a result, the crossflow in the boundary layer converged, and its profiles matched the FUN3D solutions quite well, as illustrated in Fig. 23 and as in the upper left plot of Fig. 19. All the mean flow parameters presented in Fig. 19 were obtained at time step 25,600. The kinks on the convergence curve for the current OVERFLOW computation were caused by the changes of some input parameters, such as scaling factors for artificial dissipation. Better convergence could possibly be achieved by choosing input switches more carefully.

As in Sec. III.C, three-dimensional linear stability analysis was performed here on each of the mean flows for stationary crossflow instability distributions with spanwise wavelengths of 5, 7, 9, and 11 mm along a streamline starting at the midspan location. The comparison of N factors is shown in Fig. 24 with generally good agreement for small values of x/c. However, small differences were observed in downstream regions, which may be attributed to the small differences in the mean flow profiles noted in Fig. 21.

Boundary-layer codes are widely used for generating mean flows for stability analysis for 2-D as well as 3-D wings because of their efficiency and simplicity. Therefore, the stability analysis results based, respectively, on mean flows generated by a boundary-layer solver and a Navier–Stokes solver were evaluated and compared. The boundary-layer code BLSTA was used for this purpose because it can handle not only infinite swept wings but also tapered swept wings under a spanwise conical flow assumption. Upper surface C_p along

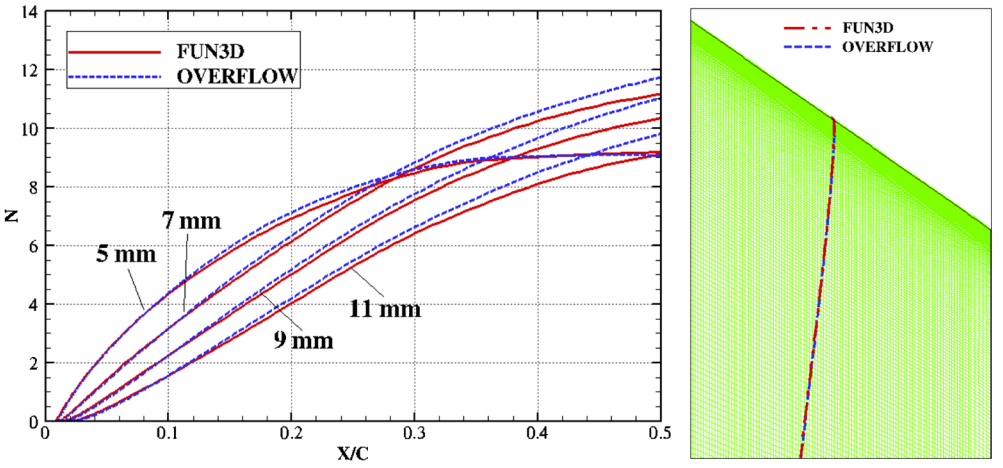

Fig. 24 3-D LST N factors based on the mean flow obtained from FUN3D and OVERFLOW solutions (left) and the corresponding streamlines along which stability analysis was conducted (right).

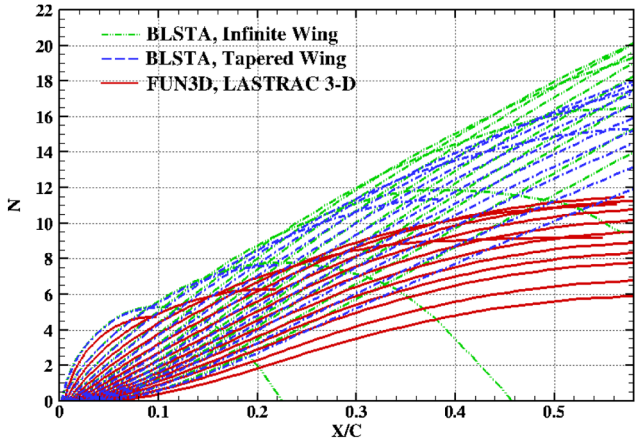

Fig. 25 Comparison of 2-D (based on quasi-3-D boundary-layer mean flows by BLSTA) and 3-D (based on Navier–Stokes mean flows by FUN3D) LST *N* factors.

the midspan of the glove was used as the boundary-layer edge condition for BLSTA. Three mean flows were generated: 1) infinite swept wing using BLSTA; 2) tapered swept wing under a spanwise conical flow assumption using BLSTA; and 3) the mean flow extracted from the FUN3D Navier–Stokes solutions. Stability computations were performed for stationary crossflow instability modes of 3 to 18 mm in wavelength, with the 3-D integration path being a streamline in case 3. The resulting N factors are shown in Fig. 25. The N factors of case 3 are only 42–57% of those of case 1, depending on spanwise wavelength. In case 2, the N factors drop 10–15% from those in case 1, whereas they are still significantly larger than those in case 3. The same computations were also conducted for the gloved-wing-only case, and similar differences were observed among the N factors based on three mean flows. It demonstrated that these differences were not related to the 3-D effects caused by the fuselage, engine, and winglet, but they were intrinsic to the glove.

The pressure distribution dominates the development of crossflow on a swept wing. We will, therefore, examine the C_p contours over the glove to find possible reasons for such a big difference between 2-D (i.e., based on quasi-3-D mean flow) and 3-D (i.e., based on 3-D Navier–Stokes mean flow) stability analysis. In Fig. 26, we illustrated the local sweep lines at $x/c = 0.3$, 0.4, and 0.6 together with C_p contours in the glove area between two span stations: $y = 204$ in. and $y = 264$ in.. It is seen that the local C_p contours are not parallel to either the leading edge or the local sweep lines. For instance,

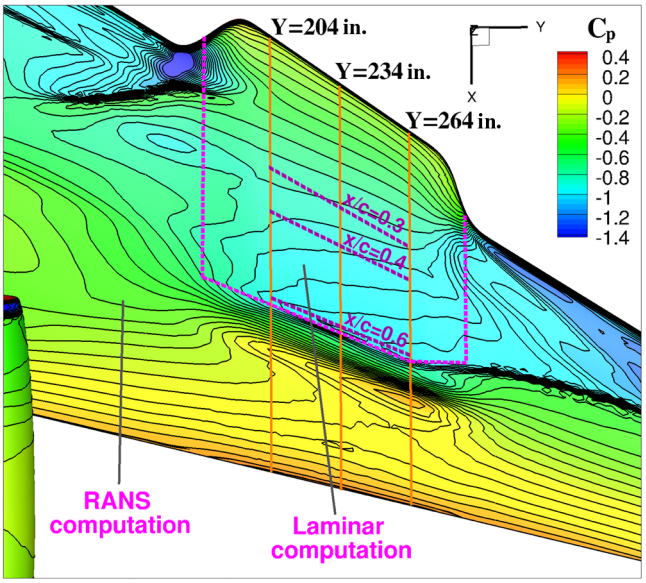

Fig. 26 C_p contours over the glove for the full G-III aircraft together with local sweep lines.

between $x/c = 0.4$ and 0.6, the actual sweep angles defined by the local C_p contours approach zero, which is much less than the sweep angle defined by the geometric sweep lines. It appears that the separation zone at the leading edge of the inboard fairing, as well as the flow along the outboard fairing, play an important role in the change of the downstream C_p distributions. The isobar unsweep in the glove region reduces crossflow, which weakens crossflow instability. A larger glove span, or perhaps a more clever design of side fairings, would have minimized this stabilizing effect. In any case, quasi-3-D boundary-layer codes (such as BLSTA) are not suitable for computing the fully three-dimensional glove boundary layer. Navier–Stokes codes, as in the present paper, or much more efficient fully 3-D boundary-layer codes [30] are needed to compute the mean flow for stability analysis. A corollary to this analysis is that design optimization based on fully three-dimensional analysis may result in more natural laminar flow than that based on quasi-3-D analysis.

IV. Conclusions

The work described in this paper was motivated by the longer-term goal of developing an efficient 3-D design capability for swept wings with laminar-flow technology. Because of the large number of design variables inherent to such applications, an adjoint-based design optimization capability becomes highly desirable in this context. The unstructured-grid flow solver FUN3D, developed at NASA Langley Research Center, includes a number of essential ingredients for the targeted capability in the form of adjoint-based optimization, built-in error estimation, and objective-based adaptive mesh refinement. However, additional effort is necessary to enable linear stability-based transition predictions for fully 3-D mean flows using unstructured-grid flow solutions.

Since the 3-D transition analysis module within the LASTRAC suite of transition analysis codes is based on boundary-layer profiles at each point of a structured-grid surface mesh, a postprocessing module is developed and implemented to interface the unstructured-grid mean flow solution from FUN3D with the LASTRAC suite of codes. The aforementioned procedure has been applied to a variety of relevant flow configurations ranging in complexity from a self-similar flat-plate boundary layer, an infinite-span swept wing, and a 3-D wing configuration to a full aircraft configuration with a gloved wing. In all of those cases, the computed mean flow solutions as well as the corresponding linear stability characteristics were compared with the predictions based on more established methods from analytical solution to solutions based on structured-grid mean flow solvers. Good agreement is observed among the results obtained by these methods. For the swept wing flow over the wing-glove assembly, it is also demonstrated that the N-factor evolution based on a full-Navier–Stokes computation differs significantly from that based on quasi-3-D boundary-layer codes owing to the unsweep of the isobars caused by the limited glove span. This points to the need for stability analysis based on Navier–Stokes solutions or possibly fully 3-D boundary-layer codes when the underlying flow develops strong three-dimensionality. Overall, the study provides some guidelines, as will be listed next, on future applications for design and analysis of complex flow configurations related to laminar-flow technology:

1) Use of first-order interpolation from unstructured-grid solutions to a structured grid used for stability analysis provides satisfactory accuracy in terms of stability related metrics, despite strong oscillations in the second derivatives of mean flow profiles. The oscillations also extend to first-order derivatives in the case of complex flow configurations such as a wing-glove assembly on an aircraft, but even then do not have a noticeable impact on the N-factor evolution for crossflow instability of the swept wing boundary layer.

2) The crossflow Reynolds number and, hence, the crossflow amplification rate as well are sensitive to mean flow convergence and may continue to evolve after typical convergence metrics related to force coefficients have well converged. Therefore, during a mean flow computation to enable stability analysis, a crossflow parameter should be monitored for convergence and, when it is not possible, the

mean flow computation should be continued until the solution residuals have dropped at least two to three orders of magnitude further beyond the stage when the overall force coefficients have converged to within typical engineering accuracy.

3) Finally, quasi-3-D boundary-layer codes, based on an infinite-span approximation or a conical-flow assumption, may not provide acceptable accuracy for stability analysis of fully 3-D boundary-layer mean flows such as those over a wing glove with $O(1)$ aspect ratios.

Acknowledgments

The current work was supported by NASA's Environmentally Responsible Aviation and Subsonic Fixed Wing projects. The authors thank Robert Biedron, James Thomas, Christopher Rumsey, and Dana Hammond of NASA Langley Research Center; and Boris Diskin of the National Institute of Aerospace for their valuable suggestions and fruitful discussions.

References

[1] Chang, C.-L., "The Langley Stability and Transition Analysis Code (LASTRAC): LST, Linear and Nonlinear PSE for 2-D, Axisymmetric, and Infinite Swept Wing Boundary Layers," AIAA Paper 2003-0974, 2003.

[2] Chang, C.-L., "LASTRAC.3d: Transition in 3D Boundary Layers," AIAA Paper 2004-2542, 2004.

[3] Chang, C.-L., and Choudhari, M., "Boundary-Layer Receptivity and Integrated Transition Prediction," AIAA Paper 2005-0526, 2005.

[4] Anderson, W. K., and Bonhaus, D. L., "An Implicit Upwind Algorithm for Computing Turbulent Flows on Unstructured Grids," *Computers and Fluids*, Vol. 23, No. 1, 1994, pp. 1–22. doi:10.1016/0045-7930(94)90023-X

[5] Anderson, W. K., Rausch, R. D., and Bonhaus, D. L., "Implicit/Multigrid Algorithms for Incompressible Turbulent Flows on Unstructured Grids," *Journal of Computational Physics*, Vol. 128, No. 2, 1996, pp. 391–408. doi:10.1006/jcph.1996.0219

[6] Nielsen, E. J., "Aerodynamic Design Sensitivities on an Unstructured Mesh Using the Navier–Stokes Equations and a Discrete Adjoint Formulation," Ph.D. Thesis, Virginia Polytechnic Inst. and State Univ., Blacksburg, VA, 1998.

[7] Lee-Rausch, E. M., Park, M. A., Jones, W. T., Hammond, D. P., and Nielsen, E. J., "Application of Parallel Adjoint-Based Error Estimation and Anisotropic Grid Adaptation for Three-Dimensional Aerospace Configurations," AIAA Paper 2005-4842, 2005.

[8] Park, M., "Low Boom Configuration Analysis with FUN3D Adjoint Simulation Framework," AIAA Paper 2011-3337, 2011.

[9] Nielsen, E. J., and Diskin, B., "Discrete Adjoint-Based Design for Unsteady Turbulent Flows on Dynamic Overset Unstructured Grids," AIAA Paper 2012-0554, 2012.

[10] Belisle, M. J., Roberts, M. W., Tufts, M. W., Tucker, A. A., Williams, T. C., Saric, W. S., and Reed, H. L., "Design of the Subsonic Aircraft Roughness Glove Experiment (SARGE)," AIAA Paper 2011-3524, 2011.

[11] Malik, M., Liao, W., Lee-Rausch, E., Li, F., Choudhari, M., and Chang, C.-L., "Computational Analysis of the G-III Laminar Flow Glove," AIAA Paper 2011-3525, 2011.

[12] Hartshorn, F., Belisle, M. J., and Reed, H. L., "Computational Optimization of a Natural Laminar Flow Experimental Wing Glove," AIAA Paper 2012-0870, 2008.

[13] Krist, S. L., Biedron, R. T., and Rumsey, C. L., "CFL3D User's Manual (Version 5.0)," NASA TM-1998-208444, 1998.

[14] Rumsey, C. L., and Lee-Rausch, E. M., "NASA Trapezoidal Wing Computations Including Transition and Advanced Turbulence Modeling," AIAA Paper 2012-2843, 2012.

[15] Nichols, R., and Buning, P., *User's Manual for OVERFLOW 2.1*, NASA Langley Research Center, Hampton, VA, 2008.

[16] Nichols, R., Tramel, R., and Buning, P., "Solver and Turbulence Model Upgrades to OVERFLOW 2 for Unsteady and High-Speed Applications," AIAA Paper 2006-2824, 2006.

[17] Ramakrishnan, R., Vatsa, V., Otto, J., and Kumar, A., "A Detailed Study of Mean-Flow Solutions for Stability Analysis of Transitional Flows," AIAA Paper 1993-3052, 1993.

[18] Garriz, J., Vatsa, V., and Sanetrik, M., "Issues Involved in Coupling Navier–Stokes Mean-Flow and Linear Stability Codes," AIAA Paper 1994-0304, 1994.

[19] Malik, M., Li, F., and Choudhari, M., "Analysis of Crossflow Transition Flight Experiment Aboard Pegasus Launch Vehicle," AIAA Paper 2007-4487, 2007.

[20] Roe, P. L., "Approximate Riemann Solvers, Parameter Vectors, and Difference Schemes," *Journal of Computational Physics*, Vol. 43, No. 2, 1981, pp. 357–372. doi:10.1016/0021-9991(81)90128-5

[21] Pirzadeh, S., "Progress Toward a User-Oriented Unstructured Viscous Grid Generator," AIAA Paper 1996-0031, 1996.

[22] Jameson, A., Schmidt, W., and Turkel, E., "Numerical Solutions of the Euler Equations by Finite Volume Methods Using Runge–Kutta Time-Stepping Schemes," AIAA Paper 1981-1259, 1981.

[23] Malik, M., "e^{Malik}: A New Spatial Stability Analysis Program for Transition Prediction Using the e^N Method," High Technology Corp. Rept. HTC-8902, Hampton, VA, 1989.

[24] Pruett, D. C., and Streett, C. L., "A Spectrally Accurate Boundary-Layer Code for Infinite Swept Wings," NASA CR-195014, 1994.

[25] Wie, Y. S., "BLSTA–A Boundary Layer Code for Stability Analysis," NASA CR-4481, 1992.

[26] Schlichting, H., and Gersten, K., *Boundary Layer Theory*, Springer, New York, 2004, p. 160.

[27] Lee-Rausch, E. M., Frink, N. T., Mavriplis, D. J., Rausch, R. D., and Milholen, R. D., "Transonic Drag Prediction on a DLR-F6 Transport Configuration Using Unstructured Grid Solvers," AIAA Paper 2004-0554, 2004.

[28] Spalart, P. R., and Allmaras, S. R., "A One-Equation Turbulence Model for Aerodynamic Flows," *La Recherche Aerospatiale*, No. 1, 1994, pp. 5–21.

[29] Anderson, D., Tannehill, J., and Pletcher, R., *Computational Fluid Mechanics and Heat Transfer*, Hemisphere, New York, 1984, pp. 121–124.

[30] Iyer, V., "Three-Dimensional Boundary-Layer Program (BL3D) for Swept Subsonic or Supersonic Wings with Application to Laminar Flow Control," NASA CR-4531, 1989.